Elsevier Editorial System(tm) for Earth and Planetary Science Letters
Manuscript Draft

Manuscript Number: EPSL-D-12-00929R1

Title: Temporal variation of methane flares in the ocean above Hydrate Ridge, Oregon

Article Type: Letters

Keywords: gas hydrates, acoustic flares, Hydrate Ridge

Corresponding Author: Dr. Anne Trehu, PhD

Corresponding Author's Institution: Oregon State Un.

First Author: Peter K Kannberg, BS

Order of Authors: Peter K Kannberg, BS; Anne Trehu, PhD; Stephen D Pierce, PhD; Charles K Paull, PhD; David W Caress, PhD

Abstract: While bubble plumes have been acoustically imaged in the water column above marine gas hydrate deposits in many studies, little is known about the temporal variation in plume intensity. In July 2008, we conducted surveys using 3.5 and 12 kHz ¬echosounders and a 75 kHz acoustic Doppler current profiler (ADCP) over the northern and southern summits of Hydrate Ridge, on the Cascadia continental margin. Our study included multiple surveys at both sites, including a survey of the northern summit that was repeated 16 times in 19 hours. Seafloor depth at the northern summit is ~600 m, well within the hydrate stability zone (HSZ), which was below ~510 m during our survey based on CTD data. Three distinct flares (a term used to denote the acoustic signature of bubble plumes) were detected at Northern Hydrate Ridge (NHR) and one was detected at Southern Hydrate Ridge (SHR), coincident with where flares were observed a decade ago, indicating that the supply of gas is stable on this time scale. High-resolution bathymetric surveys of NHR and SHR acquired with an Autonomous Underwater Vehicle (AUV) flown ~50 m above the seafloor indicate that flare locations are correlated with a distinctive pattern of short-wavelength seafloor roughness, supporting the inference of long-term stability in the location of bubble expulsion sites. As in previous studies at Hydrate Ridge, flares were not detected with the 3.5 kHz echosounder but were clearly imaged at 12 kHz. By reprocessing routine shipboard ADCP data, we show that they are also observed in at 75 kHz, indicating that a wide range of bubble sizes is present. The intensity of the flares varied strongly with time. Two primary sources for flares were observed. One, located on the regional topographic high, showed continuous activity, with two times periods of particularly strong flares that are not correlated with tidal height. The other, located on a local topographic high, shows a pulse of increased backscatter that occurred on a falling tide. While the time period of observation is not enough to constrain the effect of tidal changes in seafloor pressure on venting, the data suggest that tides are not the dominant factor controlling release of bubbles from the seafloor. The data support previously suggested models in which temporary sealing of vents by gas hydrate formation and breaking of these barriers as gas pressure builds up is responsible for "burp-like" pulses of gas expulsion. We also report the first observations of flares originating within the HSZ that extend well above the HSZ with little loss of backscatter intensity. These represent a new source of methane injection into the upper ocean and possibly the atmosphere. Flare extension above the HSZ may be due to coating of some bubbles by oil or biofilms or to inclusion of particulate matter (possibly including floating pieces of hydrate) in the plumes. Although this study provides tantalizing new information on both short-term variability in gas expulsion rate and long-term stability of vent sites, longer, well-calibrated observations that integrate

bubble flux over entire vent fields as a function of time are needed to develop accurate models for the flux of methane into the ocean and atmosphere from seafloor methane vents.

Temporal variation of methane flares in the ocean above Hydrate Ridge, Oregon

Peter K. Kannberg[1,3] , Anne M. Tréhu[1*], Stephen D. Pierce[1], Charles K. Paull[2], David W. Caress[2]

[1] College of Earth, Ocean and Atmospheric Science, Oregon State University, 104 COAS Administration Building, Corvallis, OR, 97330-, USA

[2] Monterey Bay Aquarium Research Institute, 7700 Sandholdt Road, Moss Landing, CA, 95039, USA

[3] now at: Scripps Institution of Oceanography, 9500 Gillman Dr., La Jolla, CA, 92093, USA

* Corresponding author: Anne Tréhu, College of Earth, Ocean and Atmospheric Sciences, Oregon State University, 104 COAS Administration Building, Corvallis, OR, 97330, USA; Tel: +1 541 737 2847, e-mail: trehu@coas.oregonstate.edu

Abstract:

While bubble plumes have been acoustically imaged in the water column above marine gas hydrate deposits in many studies, little is known about the temporal variation in plume intensity. In July 2008, we conducted surveys using 3.5 and 12 kHz echosounders and a 75 kHz acoustic Doppler current profiler (ADCP) over the northern and southern summits of Hydrate Ridge, on the Cascadia continental margin. Our study included multiple surveys at both sites, including a survey of the northern summit that was repeated 16 times in 19 hours. Seafloor depth at the northern summit is ~600 m, well within the hydrate stability zone (HSZ), which was below ~510 m during our survey based on CTD data. Three distinct flares (a term used to denote the acoustic signature of bubble plumes) were detected at Northern Hydrate Ridge (NHR) and one was detected at Southern Hydrate Ridge (SHR), coincident with where flares were observed a decade ago, indicating that the supply of gas is stable on this time scale. High-resolution bathymetric surveys of NHR and SHR acquired with an Autonomous Underwater Vehicle (AUV) flown ~50 m above the seafloor indicate that flare locations are correlated with a distinctive pattern of short-wavelength seafloor roughness, supporting the inference of long-term stability in the location of bubble expulsion sites. As in previous studies at Hydrate Ridge, flares were not detected with the 3.5 kHz echosounder but were clearly imaged at 12 kHz. By reprocessing routine shipboard ADCP data, we show that they are also observed in at 75 kHz, indicating that a wide range of bubble sizes is present. The intensity of the flares varied strongly with time. Two primary sources for flares were observed. One, located on the regional topographic high, showed continuous activity, with two times periods of particularly strong flares that are not correlated with tidal height. The other, located on a local topographic high, shows a pulse of increased backscatter that occurred on a falling tide. While the time period of observation is not enough to

constrain the effect of tidal changes in seafloor pressure on venting, the data suggest that tides are not the dominant factor controlling release of bubbles from the seafloor. The data support previously suggested models in which temporary sealing of vents by gas hydrate formation and breaking of these barriers as gas pressure builds up is responsible for "burp-like" pulses of gas expulsion. We also report the first observations of flares originating within the HSZ that extend well above the HSZ with little loss of backscatter intensity. These represent a new source of methane injection into the upper ocean and possibly the atmosphere. Flare extension above the HSZ may be due to coating of some bubbles by oil or biofilms or to inclusion of particulate matter (possibly including floating pieces of hydrate) in the plumes. Although this study provides tantalizing new information on both short-term variability in gas expulsion rate and long-term stability of vent sites, longer, well-calibrated observations that integrate bubble flux over entire vent fields as a function of time are needed to develop accurate models for the flux of methane into the ocean and atmosphere from seafloor methane vents.

1. Introduction:

Methane hydrates are crystalline solids that form from methane and water at low temperatures and high pressures (Sloan and Koh, 2007) and are found along continental margins wherever adequate quantities of methane and water are available. They represent a significant fraction of the total carbon reservoir and have potential implications for climate change, submarine geohazards and energy production (e.g. Kvenvolden, 1993, 2000; Kennet et al., 2000; Collett, 2002; Milkov, 2004; Westbrook et al., 2009 Shakhova et al., 2010). The hydrate stability zone (HSZ) is defined by the local temperature and pressure regime and by the chemistry of the

66 gas and the pore water (see review by Tréhu et al., 2006). Throughout most of the ocean, the
67 seafloor is within the HSZ and methane in excess of local solubility should form hydrate and
68 thus be trapped in the sediment. Plumes of bubbles that emanate from the seafloor above gas
69 hydrate deposits at many sites, however, attest to a more complex relationship between
70 subseafloor methane generation and storage and methane concentration in the ocean and
71 atmosphere (e.g. Merewether et al., 1985; Paull et al., 1995; Suess et al., 1999; Tryon et al.,
72 1999, 2002; MacDonald et al., 2002; Torres et al., 2002, 2004; Rehder et al., 2002, 2003, 2009;
73 Heeschen et al., 2003, 2005; Sauter et al., 2006).

74 Our paper contributes new observations on short (hours to days) and long (decadal) time
75 scales of variability in bubble plume activity and on the path of methane once it enters the ocean
76 above Hydrate Ridge, located ~90 km west of Newport, Oregon (Figure 1). Hydrate Ridge is
77 characterized by seafloor methane seeps, massive methane hydrate deposits near the seafloor,
78 and seismic indicators of methane hydrate and free gas in the subsurface. Many research cruises,
79 including two drilling expeditions (Ocean Drilling Program Legs 146 and 204), have been
80 conducted over the past 3 decades to better understand relationships between methane hydrates
81 and methane seeps in this environment (e.g. Davis et al., 1995; Zwart et al., 1996; Suess et al.,
82 1999; Tréhu et al., 1999, 2004a, 2006; Tryon et al., 1999, 2002; Torres et al., 2002; Brewer et al.,
83 2003; Paull et al, 2003; Claypool et al., 2006). Here and elsewhere, bubbles have been observed
84 streaming from the seafloor within the HSZ, suggesting that methane production and transport
85 rates are greater than the rate of hydrate formation and bacterially-mediated oxidation (e.g. Suess
86 et al., 1999, 2001; Heeschen et al., 2003; Tréhu et al., 2004b; Torres et al., 2002, 2004). Methane
87 gas bubbles should dissolve rapidly in the methane-undersaturated ocean (Leifer et al., 2009).
88 Inhibited dissolution, however, has been documented in a number of cases and attributed to the

presence of an armor of either oil or hydrate that isolates the methane gas from seawater (Merewether et al, 1985; MacDonald et al, 2002; Rehder et al., 2002; 2009; Solomon et al, 2009). Oil-armored bubble plumes are common in the Gulf of Mexico and allow the methane plumes to extend to sea level, releasing the methane into the atmosphere (Solomon et al, 2009). In hydrate environments, controlled experiments have shown that a hydrate armor forms almost instantaneously when a bubble enters the ocean (Rehder et al., 2002; 2009).

Methane bubble plumes in the water column can be detected using echosounders designed for mapping seafloor topography and shallow sub-seafloor structure (Merewether et al., 1985; Paull et al., 1995; Heeschen et al., 2003). In this paper, we refer to the backscatter generated by a methane plume as a "flare" because the acoustic signature resembles a flame in conventional displays of acoustic backscatter intensity. The terms "plume" and "flare" have often been used interchangeably in the literature (Hovland and Summerville, 1985). Because bubbles will resonate at a frequency that is a function of the bubble size and the densities of the gas and surrounding liquid (Clay and Medwin, 1977), a narrow-band echo sounder is sensitive to bubbles of a particular size, and multi-frequency data can provide information on the relative bubble size distribution, although the presence of hydrate armors on bubbles within the HSZ complicates quantitative analysis of bubble size.

2. Method:

Three sites with persistent flares were identified during cruises to Hydrate Ridge in the late 1990s and early 2000s (Heeschen et al., 2003, 2005). Direct observations using submersibles and remotely-operated vehicles confirmed that the flares were the result of methane bubbles emanating from the seafloor.(Suess et al., 1999; Torres et al., 2002). We had the

111 opportunity to return to these sites in July 2008 and used the 3.5 kHz and 12 kHz echosounders
112 and 75 kHz acoustic Doppler current profiler (ADCP) to determine whether the vents were still
113 active. At a water depth of 500 m, these frequencies will cause resonance of unarmored methane
114 bubbles with radii of 6.6 mm, 1.8 mm and 0.25 mm, respectively (Clay and Medwin, 1977). A
115 coating of hydrate, oil or other surfactant will affect the bubble rise rate and the size of the
116 bubbles that will resonate at a particular frequency (Leifer and Patro, 2002; Leifer and
117 MacDonald, 2003). Because the presence of such factors is likely, we cannot provide precise
118 estimates of the range of bubble sizes present. However comparison of backscatter in different
119 frequency bands can provide qualitative constraint on the distribution of large, medium and small
120 bubbles.

121 The 3.5 and 12 kHz data were acquired with the *R/V Wecoma*'s Knudson 320B/R dual-
122 frequency echosounder. No flares were observed in the 3.5 kHz data. The 12 kHz transducer is
123 a single EDO 323B with a beam width of 42 degrees, or footprint with a radius of 153 m at 400
124 m and 230 m at 600 m water depth. The line spacing of 150 m provided overlapping coverage
125 with this beam width during surveys, so that the presence or absence of flares within the survey
126 region could be detected within the entire survey area. Each survey represents a smoothed 1-hr
127 long snapshot of the distribution of venting within the survey area. Although this method for
128 obtaining a time-series of venting history or an entire vent field with an area of 1-2 km^2 has
129 limitations (discussed in detail in the next section), it provides a synoptic view of venting on a
130 spatial and temporal scale that has not previously been available for Hydrate Ridge. These data
131 should be helpful for designing future experiments to monitor bubbles in this type of
132 environment.

To increase the range of frequencies available, we also looked at raw 75 kHz ADCP data, which had been acquired as part of the core set of basic transit data using a hull-mounted Teledyne RDI Ocean Surveyor. The four ADCP beams are oriented 30 degrees away from vertical, resulting in a total beam width of 60 degrees: this implies a horizontal footprint of 890 m at 600 m water depth. While both narrowband (16m bins) and broadband (8m bins) data were collected, only broadband data were used for this study. Individual-ping relative-backscatter amplitude data were extracted from UHDAS raw binary files, using the "second_set" argument to the UHDAS "read" function (see UHDAS+CODAS data acquisition and post-processing software at http://currents.soest.hawaii.edu). Prior studies have used ADCPs to image bubbles in shallow lacustrine environments (Vagle et al., 2010), but to our knowledge this is the first use of ADCPs to image deep marine bubble plumes.

Initial acoustic surveys were performed as a series of east-west and north-south profiles above Southern Hydrate Ridge (SHR) and Northern Hydrate Ridge (NHR). An additional set of 16 repeated tracks composed of north-south oriented segments acquired in an overlapping race-track pattern were carried out over 19 hours. Ship speed during these surveys was 2-3 knots, and the output signal and recording gains were kept constant. Because of software limitations, digital data were collected in a time window corresponding to 400-800 m water depth. Because no flares had been observed to extend above the HSZ in previous studies, we expected (incorrectly) that this time window would be adequate to capture all data of interest.

To estimate relative flare intensity, backscatter return power in the 12 kHz band was summed from water depths of 575 m (just above the summit of NHR) to 510 m (the upper boundary of the HSZ; Figure 2A) and from 510 to 400 m. The log of the summed backscatter return power was then normalized to the average regional backscatter away from the plumes and

displayed in map view along the track lines as backscatter intensity in dB relative to background (Figures 2B and C). The results for the 16 consecutive tracks are displayed as a movie, with each survey representing an approximately 1-hour long “snapshot." Animation 1, showing integrated backscatter power within the HSZ (510-575 m water depth interval) and Animation 2, showing integrated backscatter power from 400-510 m water depth interval, are provided as supplementary material. Also provided are images of the flares, ordered as a function of time for each segment of the repeated survey (Figures S1-S6) and snapshots of the relative intensity in map view that comprise the frames of in the animations (Figure S7 and S8).

While there are many potential sources of acoustic backscatter in the ocean, we are confident that the near-vertical flares are due primarily to gas bubbles, with a possible additional contribution from particulate matter entrained with the bubbles. Backscatter inferred to result from organisms, both from individual marine mammals and from subhorizontal layers of zooplankton which aggregate in well defined horizontal layers with diurnal upward and downward migration (Northcote, 1964; Greenlaw, 1979), was also observed but is distinct from the near-vertical flares.

Five conductivity, temperature and depth (CTD) instrument casts were taken on the summit and flank of NHR to determine the water column temperature profile (Figure 1). These profiles were used to determine the top of the methane HSZ (Figure 3). The hydrate stability curves for different hypothetical gas compositions (Figure 3) were constructed using the Colorado School of Mines Hydrate (CSMHYD) software (Sloan and Koh, 2007).

High-resolution seafloor surveys of the crests of both SHR and NHR were conducted during two dives of an autonomous underwater vehicle (AUV) on July 17 and 18, 2009. This

AUV was developed at the Monterey Bay Aquarium Research Institute (MBARI) specifically for seafloor mapping (Kirkwood, 2007; Caress et al., 2008). The vehicle carries a Reson 7125 200-kHz multibeam sonar and collects high-resolution multibeam bathymetry (vertical precision of 0.1 m and a horizontal beam footprint of 0.75 m diameter at 50 m survey altitude). The AUV navigation and attitude derives from a Kearfott Seadevil inertial navigation system (INS) initialized by GPS at the surface and aided by a Doppler velocity log (DVL) during missions. These surveys were conducted at 3 knots with the AUV programmed to fly 50 m off the seafloor with 150 m line spacing on missions of up to 18 hours..

3. Observations and Discussion

3.1 Spatial and temporal variations in flare intensity

Horizontal spatial resolution of the acoustic data is limited by the beam width, which does not allow for precise registration of the vent site and by the possibility that bubbles are transported laterally by current. With our line spacing of ~150 m and footprint of 153 m at 400 m depth, we should have detected any flares within the survey area. Vertical resolution of the minimum depth of flares is can be underestimated if the bubbles generating the backscatter are not directly beneath the ship. We illustrate the uncertainty in the depth to the top of a flare with the example shown in Figure 12C on tracks 11-12, lines E and F near 44° 40' 12" N. The source of this flare appears to be located midway between two tracks (i.e. 75 m off the line) an apparent depth to the top of the flare of 500 m corresponds to an actual depth of 494 m. This error could potentially be as much as 30 m for a flare located outside of the survey region. Deflection of the flares by currents is not a significant source of uncertainty for this data set, as indicated by the

vertical appearance of nearly all of the flares included in this study (Figure 2A, 3C) and by the simple temperature versus depth profiles measured by the CTDs (Fig. 3A).

In 12 kHz data, three foci of flare activity were observed near the summit of NHR whereas at SHR a single distinct flare was present. All four of these sites had been active a decade earlier, as reported by Heeschen et al. (2003) and shown as grey circles in Figure 2B.

The repeated survey at NHR documented large temporal variations in relative flare intensity on a time scale of minutes to hours (Figures 2C and 3; Animations 1 and 2; Supplementary figures S1-S8). In most cases, flare intensity over a fixed spot on the seafloor varied smoothly from one track to another; however a few flares had a sharp, hyperbolic upper boundary (e.g., segment B and C in Fig. 2A). We interpret these observations to result from "burps" of methane. We attempted to estimate the rise rate of these burps but concluded that the repeat rate of our observations was too long to allow us to follow individual burps. For example, if the flares in segments B and C in Figure 2B represent backscatter from bubbles emanating from the same seafloor source, the difference in the depth to the top of the "burp" between segments B and C, which were acquired 20 minutes apart, implies a rise rate of 4.4 cm/s, which is unrealistically slow compared to the rise rate of 26-29 cm/s found by others for bubbles at SHR (Rehder et al., 2002; Brewer et al., 2002). Although it is likely that we missed some "burbs" because of a repeat rate that was slower than the time it takes for a "burp" to move from the seafloor to the top of the HSZ, clear variability on an hourly time scale is visible in the data and "burps" seem to be followed by a period of increased backscatter with a time scale >1 hour. A long-term monitoring system focused on a single plume would be needed to monitor the temporal evolution of individual "burps."

Flares observed in the 75 kHz data were collocated with flares observed at 12 kHz but showed significantly less spatial and temporal variability (Figure 4, upper right) as well as a much wider "footprint" due to the wider beam width of the source. Backscatter return amplitude fell off very quickly with height above the seafloor and reached background levels well below the upper limit of the HSZ. This could potentially be due to more rapid dissolution of the smaller bubbles detected with 75 kHz (Rehder et al., 2009).

3.2. Correlation between flares and seafloor topography

A general correlation between current or past venting and rough seafloor topography that results from the presence of slabs and chimneys of authigenic carbonate has been recognized since the pioneering observations of Kulm et al. (1986). We refine this correlation by documenting variations in the fine-scale roughness that are revealed by high-resolution bathymetry acquired by an AUV. These observations suggest that fine-scale roughness has the potential provide new constraints on the temporal history of venting. At NHR, the three regions of high flare activity correspond to relative bathymetric highs characterized by distinctive fine-scale roughness (Figure 4A). The correlation between active venting and roughness is particularly apparent in maps of the amplitude of the local seafloor slope vector, determined by differencing adjacent bathymetric values to find the steepest path (Figure 4B). The seafloor photographs show changes in the seafloor corresponding to different seafloor slope characteristics. All four of the images fall within the region characterized by methane venting as indicated by the proxies of seafloor baterial mats, macrofauna, and carbonates. However only Image 3 falls within the region characterized by vigorous expulsion of free gas and by fine-scale

roughness. A similar correlation is observed at SHR (Figure 5), although here flares were only observed over the summit (Figure 5A), where the seafloor is hummocky and the sediments contain ~20% massive gas hydrate by volume but little carbonate in the upper 40 m below the seafloor (Tréhu et al., 2004a). We suggest that the correlation between hummocky, rough terrain and venting results from re-suspension of sediment by upward gaseous flow, possibly enhanced by aqueous flow. Existing data indicate temporal changes in the rate of aqueous in-flow and out-flow in this region (Tryon et al., 1999, 2002); however, the spatial distribution of measurement is very limited. Additionally, buoyant hydrate blocks could potentially remove sediment grains that adhere to the blocks (Paull et al. 1995), contributing to the roughness. This hypothesis could be tested by future experiments to measure flow rate across the boundary between rough and smooth seafloor while simultaneously acoustically imaging the water column.

The association between high seafloor roughness and bubble plumes, however, is imperfect as we note that the pinnacle region of SHR is also characterized by high seafloor roughness. Fluids exiting the pinnacle contain dissolved methane but no acoustic flare or bubbles have been observed in spite of multiple crossings (e.g. Torres et al., 2002; Tryon et al., 2002). Seafloor roughness on NHR also extends north and south of where flares have been observed. With the exception of the region circled in red in Figure 4B, the regions of high seafloor roughness but no bubbles show systematic NE or NW-trending lineations, in contrast to the short spatial scale and lack of coherent directional trends in the rough zones corresponding to flares. We speculate that these morphological differences reflect differences in the underlying plumbing system that may reflect evolution of venting processes on longer time scales. The region outlined by a red circle on Figure 4B, which is characterized by high roughness in a local topographic

depression, may be where a former gas storage chamber collapsed. A similar process may explain the apparent moat encircling the Pinnacle at SHR.

3.3 Tidal correlation

Temporally variable methane bubble flux from NHR has been noted in previous studies based on intermittent observations of bubbles from an ROV or submersible (Suess et al., 1999; Tryon et al., 1999; Torres et al., 2002). Torres et al. (2002) suggested that the bubble flux at the summit of North Hydrate Ridge might be mediated by tidal loading based on two observations of low bubble flux during high tide and six observations of higher flux during low tide over a 3-day period. Our repeated survey of NHR (Figure 2C) took place two days after a new moon, during a neap tide so that the amplitude of tidal change was relatively large. Figure 6 shows relative flare intensity in discrete time windows estimated by summing the backscatter power for each of the 16 tracks recorded during the repeated survey compared to the barotropic tidal variation at 44° 40.0’ N 125° 06.0’ W, calculated using the Oregon State University Tidal Inversion Software (Egbert and Erofeeva, 2002). The histogram indicates the total average backscatter within the large rectangle of Figure 2C, with dark grey indicating backscatter within the box labeled 6NE, which encompasses the summit of NHR, and lighter grey indicating the backscatter from the rest of the region. No correlation with tides is observed for the entire survey or for the subset of the region that includes the vents at the NHR summit, which peaked during both high and low tide. Discrete methane "burps" southwest of the summit (e.g. segment C on track 11 in Figure 2) were more frequent during the decreasing tide on July 6, although we do not see any evidence for an

increase in backscatter immediately after the tidal minimum on July 15; we cannot tell whether this apparent correlation is causal or coincidental.

While our time series is too short to provide a definitive answer to the question of whether tides influence venting, the data indicate that tides are not the primary factor controlling the flux of bubbles from the seafloor. If tidal pressure were the primary factor, assuming a gas source region 100 m beneath the seafloor, the predicted lag between tidal pressure at the seafloor and flare observations would be ~10 minutes (Wang and Davis, 1996). This lag is too short to be resolved by our data, so the highest flux would be correlated with the lowest tide and vice versa, assuming that gas travels rapidly from the source to the seafloor (Torres et al., 2002). The data do, however, allow for a correlation between discrete gaseous "burbs" southwest of the NHR summit and decreasing tidal pressure on the seafloor. Our observations are thus consistent with the model in which the bubble flux is controlled primarily by temporary sealing of vents by hydrate formation and by the subsequent release of gas after the gas pressure rises and breaks the seal, as originally proposed by Tryon et al. (1999, 2002) for NHR and more recently by Bangs et al. (2011) and Daigle et al. (2011) for SHR. Longer time series are needed to reveal the possible impact of intermittent tectonic events, like earthquakes, as well as to resolve whether tides modulate the bubble flux.

3.4 Extension of flares above the HSZ

While our results generally support past findings that indicate rapid bubble dissolution above the HSZ, three flares clearly extended above the HSZ at NHR (Figures 2, 3, 4, Animation 2). Of these extended flares, two show decreasing backscatter strength as they near the ceiling of our sample window at 400 m depth. One flare however, shows no measurable decrease in

backscatter between the top of the methane HSZ and the top of our recording window at 400 m depth (Figure 7).

This is the first time flares have been reported to extend above the methane HSZ at Hydrate Ridge and is important because methane bubble plumes are a poorly quantified contributor to atmospheric methane (Solomon et al, 2009). If these plumes extend into the mixing zone, they represent a pathway for subseafloor methane to ventilate to the atmosphere because oceanic methane oxidation rates are much slower than mixing zone ventilation rates. Additionally, methane that is oxidized in the ocean below the mixing zone increases ocean acidity and decreases dissolved oxygen (Valentine et al, 2001). Determining the frequency of such events at Hydrate Ridge will require longer continuous observations.

We consider five explanations for these observations and conclude that three are unlikely and that two are possible. First we hypothesize that the bubbles responsible for this anomalous flare contained enough carbon dioxide and ethane to perturb the HSZ enough to let armored bubbles rise to less than 400 mbsl. While the hydrocarbon source at Hydrate Ridge is predominantly biogenic, both ODP legs 146 and 204 found some evidence of mixed thermogenic and biogenic source gas containing higher order hydrocarbons (Westbrook et al., 1994; Hovland et al., 1995; Tréhu et al., 2003; Claypool et al., 2006). Perturbations of the HSZ were calculated based on gas concentrations in void gas samples from leg 146 at NHR (Sloan and Koh, 2007). For a gas composition of 2% carbon dioxide, 4% ethane, and 94% methane, the upper limit of the HSZ would rise ~70 meters above the pure methane stability boundary (Figure 2). While the composition of the gas that would be needed to raise the upper limit of the HSZ to 400 m is not unique, possible compositions range from 95% methane, 5% ethane and 0% carbon dioxide to

68% methane, 0% ethane and 32% carbon dioxide. Such high concentrations of ethane and carbon dioxide are considered to be unlikely based on data from ODP Legs 146 and 204.

Next we considered entrainment of colder, deeper water with the bubble plume. Sauter et al. (2006) found that iso-temperature and salinity contours were shifted upward ~100 m inside bubble plumes. While entrainment may transport dissolved methane to depths above the HSZ, a 100 m upward shift in the temperature profile at NHR would only result in a 10 m upward shift in the HSZ. Entrainment of cold water is therefore not a likely explanation for our observations.

Ebullition in response to decreasing water pressure is a third potential mechanism for bubble presence above the HSZ. Water samples taken above Hydrate Ridge show elevated dissolved methane concentrations both within and above the HSZ (Seuss et al. 1999). However these concentrations are well below saturation, making the possibility of ebullition at Hydrate Ridge unlikely.

A fourth explanation is that some of the bubbles were armored by oil or biological surfactants that protect them from dissolution. Oil-armored bubbles have been observed in the Gulf of Mexico and slow the rate of bubble dissolution (MacDonald et al., 2002; Leifer and MacDonald, 2003). However, there is little evidence for liquid hydrocarbons at NHR (Hovland et al., 1995). Biofilms are another possible bubble coating. Leifer and Patro (2002) showed that polymucosaccharides have a similar affect on bubbles as oil. Rise rates of unarmored bubbles should slow over time as the radius of the bubbles, and consequently their buoyancy, decreases due to dissolution. Salmi et al. (2011) concluded that nearly constant rise rates of bubbles from a methane vent in approximately 150 m of water on the continental margin of Washington might be due to armoring of bubbles by biofilms as the bubbles pass through bacterial mats. Biofilms

have recently been found in association with bacterial mats and gas hydrates in several regions (Briggs et al., 2011).

A fifth explanation is that these bubble plumes contained solid pieces of hydrate that broke loose from the seafloor. If the hydrate chunks were large enough, they would start dissociating and releasing bubbles as they rose through upper boundary of the HSZ (Paull et al. 2003). These chunks of hydrate, which would not show the same frequency-dependent resonance as bubbles because of the stiffness of the hydrate, would be masked by the resonant bubbles within the HSZ, explaining why the plumes that rise above the HSZ are not significantly more reflective than other plumes when below the HSZ (Figure 7, Animation 1). Brewer et al. (2002) and Paull et al. (2003) predicted and observed such behavior on prior expeditions.

4. Conclusions:

Many acoustic surveys have been conducted around the world to detect the existence of acoustic flares resulting from bubble plumes, but none have provided the long time series needed to monitor changes in methane flux. Consequently, little is known about temporal variability in methane flux. The survey reported here, which documents a return to sites observed a decade ago as well as providing a 19-hour time series at a vigorous venting site, provides a tantalizing first look at temporal and spatial variations in the rate of methane flux from the seafloor. Conclusions from our observations include:

- Expulsion of free gas from the summits of Northern and Southern Hydrate Ridge, as monitored by observations of acoustic flares, is spatially and temporally persistent on decadal time scales.

- Disappearance of most flares at 510 m, the depth to the top of the methane hydrate stability boundary, supports previous models in which bubbles are armored by hydrate, thus delaying dissolution.
- Flare intensity at 12 kHz varies strongly with time on an hourly time scale, suggesting intermittent release of gas on this time scale; this temporal variation was not correlated with tidal pressure on the seafloor. Less temporal or spatial variation was observed in 75 kHz data and no flares were observed at 3.5 kHz. Our observations support a model for expulsion of free gas in which subsurface gas migration pathways are are blocked by hydrate formation and and that these seal rupture as gas pressure increases, as previously suggested by Tryon et al. (1999, 2002) for NHR and by Bangs et al. (2011) and Daigle et al. (2011) for SHR. Subtle tidal modulation of gas flow, however, cannot be ruled out by our observations.
- For the first time at Hydrate Ridge, some flares were observed to extend well above the top of the hydrate stability zone. These observations may result from dissociation of solid hydrate pieces entrained with the bubble plume or from coating of some bubbles by oil or biofilms prior to emergence from the seafloor. Perturbation of the ocean temperature by entrainment of cold water, the effect of higher order hydrocarbons on the stability curve, or ebullition in response to decreasing pressure are considered to be unlikely explanations for this observation. We cannot tell from our observations the frequency of injection of gas into the ocean above the HSZ, and possibly into the atmosphere, from vents located within the HSZ. This could be a very rare event that we captured serendipitously
- Source regions for flares are characterized by incoherent, small-scale seafloor roughness. While the rough area extends beyond the source region for the flares, the character of the roughness shows subtle changes that may reflect temporal evolution of venting.

Acknowledgments

We thank the captain and crew of the *R/V Wecoma* for cheerfully driving the ship in circles for hours. Darryl Swenson provided able technical assistance during the cruise. Jochen Braunmiller, Mark Williams and Jeremy Childress stood watch during the 12 kHz surveys. Many of the figures were made using GMT (Wessel and Smith, 1998). Data acquisition was supported by NSF grant OCE-0550402 and analysis was supported by OCE-0646226. The David and Lucile Packard Foundation provided the support for the high-resolution multibeam data collection. The manuscript benefitted from comments by 3 anonymous reviewers.

References:

Bangs, N.L., Hornbach, M.J., Berndt, C., 2011. The mechanics of intermittent methane venting at South Hydrate Ridge inferred from 4D seismic surveying, Earth Plan. Sci. Lett., 310(1-2), 105-112, doi:10/1016/j.epsl.2011.06.022.

Brewer, P.G., Paull, C.K., Peltzer, E.T., Ussler III, W., Rehder, G., Friederich G., 2002. Measurement of the fate of gas hydrates during transit through the ocean water column. Geophys. Res. Lett. 29. doi:10.1029/2002GL014727.

Briggs, B.R., Pohlman, J.W., Torres, M., Riedel, M., Brodie, E.L., Colwell, F.S., 2011. Macroscopic biofilms in fracture-dominated sediment that anaerobically oxidize methane. Appl. Environ. Microbiol. 77, 6780-6787. doi:10.1128/AEM.00288-11.

Caress, D.W., Thomas, H., Kirkwood, W.J., McEwen, R., Henthorn, R., Clague, D.A., Paull, C.K., Paduan, J., Maier, K.L., 2008. High-resolution multibeam, sidescan, and subbottom surveys using the MBARI AUV D. Allan. B, in: Reynolds, J.R., Greene, H.G. (Eds.), Marine Habitat Mapping Technology for Alaska. Alaska Sea Grant College Program, Univ. Alaska Fairbanks, pp. 47-69. doi:10.4027/mhmta.2008.04.

Clague, D., Maher, N., Paull, C.K., 2001. High resolution multibeam survey of Hydrate Ride, Offshore Oregon. In: Paull, C.K., Dillon, W.B (Eds.), Natural Gas Hydrates, Occurrence, Distribution and Detection, Geophysical Monograph, vol. 124, American Geophysical Union, pp. 41-52.

Clay, C.S., Medwin, H., 1977. Acoustical Oceanography, John Wiley, New York.

Claypool, G.E., Milkov, A.V., Lee, Y.-J. Torres, M.E., Borowski, W.S., Tomaru, H., 2006. Microbial methane generation and gas transport in shallow sediments of an accretionary complex, southern Hydrate Ridge (ODP Leg 204), offshore Oregon, USA, in: Tréhu, A.M., Bohrmann, G., Torres, M.E., Colwell, F.S. (Eds.), Proc. Ocean Drill. Prog. Sci. Results 204. College Station, TX (Ocean Drilling Program), pp. 1-52. doi:10.2973/odp.proc.sr.204.113.2006.

Collett, T.S., 2002. Energy resource potential of gas hydrates. Am. Assoc. Pet. Geol. Bull. 86(11), 1971-1992. doi: 10.1306/61EEDDD2-173E-11D7-8645000102C1865D.

Daigle, H., Bangs, N.L., Dugan, B., 2011, Transient hydraulic fracturing and gas release in methane hydrate settings: A case study from southern Hydrate Ridge, Geochem. Geophys. Geosystems, 12(12), 15 pp., doi:10.1029/2001GC003841.

Davis, E.E., Becker, K., Wang, K., Carson, B., 1995, Long-term observations of pressure and temperature in Hole 892B, Cascadia accretionary prism, in: Carson, B., Westbrook, G.K., Musgrave, R.J., Suess, E., (Eds.), Proc. Ocean Drill. Prog. Sci. Results 146. College Station, TX (Ocean Drilling Program), p. 299-311.

Egbert, G.D., Erofeeva, S.Y., 2002. Efficient inverse modeling of barotropic ocean tides. J. Atmos. Oceanic Technol. 19(2), 183-204.

Greenlaw, C.F., 1979. Acoustical estimation of zooplankton populations. Limnol. Oceanog. 24(2), 226-242.

Heeschen, K.U., Tréhu, A.M., Collier, R.W., Suess, E., Rehder, G., 2003. Distribution and height of methane bubble plumes on the Cascadia Margin characterized by acoustic imaging. Geophys. Res. Lett. 30. doi:10.1029/2003GL016974.

Heeschen, K.U., Collier, R.W., de Angelis, M.A., Suess, E., Rehder, G., Linke, P., Klinkhammer G.P., 2005. Methane sources, distributions, and fluxes from cold vent sites at Hydrate Ridge, Cascadia Margin. Global Biogeochem. Cycles 19, GB2016. doi:10.1029/2004GB002266.

Hovland, M., Sommerville J.H., 1985. Characteristics of two natural gas seepages in the North Sea. Mar. Petrol. Geol. 2(4), 319-326.

Hovland, M., Lysne, D., Whiticar M.J., 1995. Gas hydrate and sediment gas composition, ODP Hole 892A, offshore Oregon, USA, in: Carson, B., Westbrook, G.K., Musgrave, R.J., Suess, E., (Eds.), Proc. Ocean Drill. Prog. Sci. Results 146. College Station, TX (Ocean Drilling Program), pp. 151-161.

Kennet, J.P., Cannariato, K.G., Hendy, I.L., Behl R.J., 2000. Carbon isotopic evidence for methane hydrate instability during quaternary interstadials. Science 288, 128-133.

Kirkwood, W.J., 2007. Development of the DORADO mapping vehicle for multibeam, subbottom, and sidescan science missions. J. Field Robot. 24, 487-495.

Kulm, L.D., Suess, E., Moore, J.C., Carson, B., Lewis, B.T., Ritger, S.D., Kadko, D.C., Thornburg, T.M., Embley, R.W., et al., 1986, Oregon subduction zone: venting, fauna and carbonates, Science, 231(4738) 561-566, doi:10.1126/science.231.4738.561.

Kvenvolden, K.A., 1993. A primer on gas hydrates, in: Howell, D.G. (Ed.), United States Geological Survey Professional Paper 1570, 279-292.

485 Kvenvolden, K.A., 2000. Natural gas hydrate: introduction and history of discovery, in: Max,
486 M.D., (Ed.), Natural Gas Hydrate in Oceanic and Permafrost Environments. Kluwer,
487 Massachusetts, pp. 9-16.
488
489 Leifer, I., Patro, R.K., 2002. The bubble mechanism for methane transport from the shallow sea
490 bed to the surface: A review and sensitivity study. Continental Shelf Res., 22, 2409-2428,
491 doi:10.1016/S0278-4343(02)00065-1.
492
493 Leifer, I., MacDonald, I., 2003. Dynamics of the gas flux from shallow gas hydrate deposits:
494 interaction between oily hydrate bubbles and the oceanic environment. Earth Planet. Sci. Lett.
495 210(3-4), 411-424. doi: 10.1016/S0012-821X(03)00173-0.
496
497 Leifer, I., Jeuthe, H., Gjosund, S.H., Johansen, V., 2009. Engineered and natural methane seep,
498 bubble-driven buoyancy flows. J. Phys. Oceanogr. 39(12), 3071-3090.
499
500 MacDonald, I.R., Leifer, I., Sassen, R., Stine, P., Mitchell, R., Guinasso Jr., N., 2002. Transfer of
501 hydrocarbons from natural seeps to the water column and atmosphere. Geofluids 2(2), 95-107.
502
503 Merewether, R., Olsson, M.S., Lonsdale, P., 1985. Acoustically detected hydrocarbon plumes
504 rising from 2-km depths in Guaymas Basin, Gulf of California. J. Geophys. Res. 90(B4), 3075-
505 3085.
506
507 Milkov, A.V., 2004. Global estimates of hydrate-bound gas in marine sediments: how much is
508 really out there? Earth Sci. Rev. 66, 183-197.
509
510 Northcote, T.G., 1964. Use of a high-frequency echo sounder to record distribution and
511 migration of Chaoborus larvae. Limnol. Oceanogr. 9(1), 87-91.
512
513 Paull, C. K., Ussler, W., Borowski, W.S., Spiess F.N., 1995. Methane-rich plumes on the
514 Carolina continental rise: Associations with gas hydrates. Geology 23(1), 89-92.
515 doi:10.1130/0091-7613(1995)023<0089:MRPOTC>2.3.CO;2.

Paull, C.K., Brewer, P.W., Ussler, W., Peltzer, E.T., Rehder, G., Claque, D., 2003. An experiment demonstrating that marine slumping is a mechanism to transfer methane from the seafloor gas-hydrate deposits into the upper ocean and atmosphere. Geo. Mar. Lett. 22(4), 198-203.

Rehder, G., Brewer, P.W., Peltzer, E.T., Friederich, G., 2002. Enhanced lifetime of methane bubble streams within the deep ocean. Geophys. Res. Lett. 29. doi:10.1029/2001GL013966.

Rehder, G., Collier, R.W., Heeschen, K., Kosro, P.M., Barth, J., Suess, E., 2003. Enhanced marine CH_4 emissions to the atmosphere off Oregon caused by coastal upwelling. Global Biogeochem. Cycles 16(3) 1081. doi:10.1029/2000GB001391.

Rehder, G., Leifer, I., Brewer, P.G., Friederich, G., Peltzer, E.T., 2009. Controls on methane bubble dissolution inside and outside the hydrate stability field from open field experiments and numerical modeling. Mar. Chem. 114, 19-30.

Salmi, M.S., Johnson, H.P., Leifer, I., Keister, J.E., 2011. Behavior of methane seep bubbles over a pockmark on the Cascadia continental margin. Geosphere, 7, 1273-1283, doi:10.1130/GES00648.1.

Sauter, E. J., Muyakshin, S.I., Charlou, J., Schlüter, M., Boetius, A., Jerosch, K., Damm, E., Foucher, J., Klages, M., 2006. Methane discharge from a deep-sea submarine mud volcano into the upper water column by gas hydrate-coated methane bubbles. Earth Planet. Sci. Lett. 234(3-4), 354-365.

Shakhova, N., Semiletov, I., Salyuk, A., Yusupov, V., Kosmach, D., Gustafsson, Ö., 2010. Extensive methane venting to the atmosphere from sediments of the East Siberian Arctic Shelf. Science 327 (5970), 1246. doi: 10.1126/science.1182221.

Sloan, E.D., Koh, C., 2007. Clathrate hydrates of natural gases, third ed. CRC Press, Florida.

Solomon, E.A., Kastner, M., MacDonald, I.R., Leifer, I., 2009. Considerable methane fluxes to the atmosphere from hydrocarbon seeps in the Gulf of Mexico. Nat. Geosci. 2(8), 561-565.

Suess, E., Torres, M.E., Bohrmann, G., Collier, R.W., Geinert, J., Linke, P., Rehder, G., Tréhu, A., Wallmann, K., Zuleger, E., 1999. Gas hydrate destabilization: enhanced dewatering, benthic material turnover and large methane plumes at the Cascadia convergent margin. Earth Planet. Sci. Lett. 170, 1-15.

Suess, E., Torres, M.E., Bohrmann, G., Collier, R.W., Rickert, D., Goldfinger, C., Linke, P., Heuser, A., Sahling, H., Heeschen, K., Jung, C., Nakamura, K., Greinert, J., Pfannkuche, O., Tréhu, A., Klinkhammer, G., Whiticar, M.J., Eisenhauer, A., Teichert, B., and Elvert, M., 2001. Sea floor methane hydrates at Hydrate Ridge, Cascadia margin, in: Paull, C.K., Dillon, W.P. (Eds.), Natural gas hydrates: occurrence, distribution, and detection, Geophysical Monograph, vol. 124, American Geophysical Union, pp. 87–98.

Torres, M.E., McManus, J., Hammond, D.E., de Angelis, M.A., Heeschen, K.U., Colbert, S.L., Tryon, M.D., Brown, K.M., Seuss, E., 2002. Fluid and chemical fluxes in and out of sediments hosting methane hydrate deposits on Hydrate Ridge, OR, I: Hydrologic provinces. Earth Planet. Sci. Lett. 201, 525-540.

Torres, M.E., Wallman, K., Tréhu, A.M., Bohrmann, G., Borowski, W.S., Tomaru, H., 2004. Gas hydrate growth, methane transport, and chloride enrichment at the southern summit of Hydrate Ridge, Cascadia margin off Oregon. Earth Planet. Sci. Lett. 226, 225-241.

Tréhu, A.M., Torres, M.E. Moore, G.F., Seuss, E., Bohrmann, G., 1999. Temporal and spatial evolution of a gas hydrate-bearing Accretionary ridge on the Oregon continental margin. Geology v. 27 no. 10 p. 939-942

Tréhu, A.M., Bohrmann, G., Torres, M.E., Colwell, F.S. (Eds.) 2003. Proc. Ocean Drill. Prog. Init. Reports 204. College Station, TX (Ocean Drilling Program). doi:10.2973/odp.proc.ir.204.2003.

Tréhu, A.M., Bohrman, G., Rack, F.R., Collett, T.S., Goldberg, D.S., Long, P.E., Milkov, A.V., Riedel, M., Schultheiss, P., Torres, M.E., Bangs, N.L., Barr, S.R., Borowski, W.S., Claypool, G.E., Delwiche, M.E., Dickens, G.R., Gracia, E., Guerin, G., Holland, M., Johnson, J.E., Lee, Y-J., Liu, C-S., Su, X., Teichert, B., Tomaru, H., Vanneste, M., Watanabe, M., Weinberger, J.L., 2004a. Three-dimensional distribution of gas hydate beneath southern Hydrate Ridge: constraints from ODP Leg 204. Earth Planet. Sci. Lett. 222, 845-862.

Tréhu, A.M., Flemings, P., Bangs N., Chevallier, J., Gracia, E., Johnson, J., Riedel, M., Liu, C-S, Liu, X., Riedel, M., Torres, M.E., 2004b. Feeding methane vents and gas hydrate deposits at south Hydrate Ridge. Geophys. Res. Lett. 31, L23310. doi:10.1029/2004GL021286.

Tréhu, A.M., Ruppel, C., Holland, M., Dickens, G.R., Torres, M., Collett, T.S., Goldberg, D., Riedel, M., Schultheiss, P., 2006. Gas hydrates in marine sediments: lessons from scientific ocean drilling. Oceanography 19(4), 124-142.

Tryon, M.D., Brown, K.M., Torres, M.E., Tréhu, A.M., McManus, J., Collier, R.W., 1999, Measurements of transience and downward fluid flow near episodic methane vents, Hydrate Ridge, Cascadia, Geophys. Res. Lett., 27(12), 1075-1078.

Tryon, M., Brown, K., Torres, M., 2002. Fluid and chemical flux in and out of sediments hosting methane hydrate deposits on Hydrate Ridge, OR, II: Hydrological processes. Earth Planet. Sci. Lett. 201(3-4), 541-557. doi: 10.1016/S0012-821X(02)00732-X.

Vagle, S., Hume, J., McLaughlin, F., MacIsaac, E., Shortreed, K., 2010. A methane bubble curtain in meromictic Sakinaw Lake, British Columbia. Limnol. Oceanogr. 55(3), 1313-1326.

Valentine, D. L., Blanton, D.C., Reeburgh, W.S., Kastner, M., 2001. Water column methane oxidation adjacent to an area of active hydrate dissociation, Eel River Basin. Geochim. Cosmochim. Acta 65, 2633-2640.

609 Wang, K., Davis, E.E., 1996. Theory for the propagation of tidally induced pore pressure
610 variations in layered sub seafloor formations. J. Geophys. Res. 101(B5), 11483-11495.
611
612 Westbrook, G.K., Carson, B., Musgrave, R.J., et al. 1994. Proc. Ocean Drill. Prog. Init. Reports
613 146 (Part 1). College Station, TX (Ocean Drilling Program). doi:10.2973/odp.proc.ir.146-1.1994.
614
615 Westbrook, G. K., Thatcher, K.E., Rohling, E.J., Piotrowski, A.M., Paelike, H. Osborne, A.H.,
616 Nisbet, E.G., Minshull, T.A., Lanoiselle, M., James, R.H., Huehnerbach, V., Green, D., Fisher,
617 R.E., Crocker, A.J., Chabert, A., Bolton, C., Beszczynska-Moeller, A., Berndt, C., Aquilina, A.,
618 2009. Escape of methane gas from the seabed along the West Spitsbergen continental margin.
619 Geophys. Res. Lett. 36, L15608. doi:10.1029/2009GL039191.
620
621
622 Wessel, P., Smith, W.H.F., 1998. New, improved version of Generic Mapping Tools released,
623 EOS Trans. Amer. Geophys. U., 79 (47), p. 579.
624
625 Zwart, G., Moore, J.C., Cochrane, G.R., 1996. Variations in temperature gradients identify active
626 faults in the Oregon accretionary prism. Earth Planet. Sci. Lett. 139(3-4), 485-495. doi:
627 10.1016/0012-821X(95)00244-7.
628

Figure Captions:

Figure 1. Bathymetric map of Hydrate Ridge after Clague et al. (2001). Star in the inset shows geographic location. NHR and SHR indicate the summits of Northern and Southern Hydrate Ridge. Grey dots aligned along 48°39'N are locations of CTD casts taken during *R/V Wecoma* cruise W0807A and shown in Figure 3. Black dots indicate drill sites during ODP Legs 146 and 204.

Figure 2. (A) Track 11 from the repeated 12 kHz survey on NHR. Backscatter power was integrated from just above the seafloor at 575 m to the top of the hydrate stability zone at 510 m and plotted with a logarithmic scale normalized to the background backscatter power away from the flares. The backscatter power is also color-coded with the same palette used for displaying the data in map view in (B) and (C). A, B, C, D, E, and F correspond to survey segments shown on track 11 in C. (B) Comparison of flare locations on Northern Hydrate Ridge (NHR) and Southern Hydrate Ridge (SHR) in 2008 with flare locations in 1998-2000, which are shown as grey ellipses from Heeschen et al (2003). The colored overlay shows the relative backscatter power calculated as shown in (A). (C) Four consecutive tracks from the repeated survey on NHR. Beam width of 460 m at 510 m depth results in overlap between adjacent segments of each track. For the entire sequence, see the animations and the supplementary figures. The boxes labeled 6NE and 6SW on track 10 show the regions included in the summed backscatter graphs in Figure 6.

Figure 3. (A) Hydrate stability curves at Hydrate Ridge calculated using Colorado School of Mines Hydrate software (CSMHYD) (Sloan and Koh, 2007) for 3 different hydrate compositions based on void gas samples taken during ODP Leg 146 at site 892 on North Hydrate Ridge

(Westbrook et al., 1994). Blue denotes pure methane in seawater. Green represents the average void gas composition at ODP site 892. Red is the maximum ethane and carbon dioxide concentrations found. Black lines are from CTD casts taken in July 2008 near the summit of NHR (see Figure 1 for locations). The temperature profile of the water column intersects the pure methane and seawater curve at a depth of ~510m. (B) 75 kHz ADCP data for the same time period. All flares are clearly visible in both the 12 kHz and the 75 kHz. Flares appear wider in the 75 khz ADCP plot due to a wider beam width. (C) 12 kHz backscatter for track 15. The beam width for the 12 and 75 kHz data is also shown.

Figure 4. (A) High-resolution bathymetric map of Northern Hydrate Ridge. Red line indicates the TOWCAM trace, with numbers corresponding to the location of pictures 1-4 in (C). (B) Magnitude of the local seafloor slope vector. Yellow circles indicate flare sites. Red circle indicates a region of high roughness associated with a relative topographic low. (C) TOWCAM photographs 1-4 show how the seafloor character changes from the flank to the summit of NHR.

Figure 5. (A) High-resolution bathymetric map of Southern Hydrate Ridge with summit and pinnacle regions labeled. (B) Magnitude of the seafloor slope vector. Circle delineates the location of the flare. (C) Photographs showing the seafloor character at the summit and at the pinnacle.

Figure 6. Tidal height (black line) and summed backscatter power (grey histogram) for each of the 16 tracks completed over North Hydrate Ridge. Width of the bar indicates the time it took to complete the track, which varied slightly. The histogram indicates the total average backscatter within the large rectangle in Figure 2C, with dark grey indicating backscatter within the box labeled 6NE and lighter grey showing the rest of the region. Numbers in white indicate the track

673 number. Tide at 44 40.0 N 125 06.0W was calculated using the Oregon State University Tidal
674 Inversion Software (Egbert and Erofeeva, 2002).

675 Figure 7. Relative backscatter power for track 15. The horizontal line at 510 m is the upper limit
676 of the HSZ. Relative backscatter power within the highlighted areas was summed over 15m
677 vertical depth bins, shown by the dark grey histograms to the right of each highlighted area. The
678 bottom 1-2 samples represent backscatter from the seafloor. The flare on the right maintains
679 constant backscatter strength from the top of the HSZ at 510 m to the survey ceiling at 400 m.
680

681 Animation 1. Animation showing consecutive tracks of the repeated acoustic survey at NHR.
682 The acoustic backscatter is integrated from just above the summit of NHR to the upper boundary
683 of the HSZ, at 510 meters below sea level (mbsl) and shown with a logarithmic color scale (see
684 Figure 2 for normalized scale annotations in dB). Red is high backscatter, interpreted as high
685 bubble density, and greens and blues indicate low backscatter, indicating low bubble density.
686 Tidal height at NHR is shown on the left side of the animation, with the red bar indicating the
687 time of the displayed track.

688 Animation 2. Animation of the same survey shown in Animation 1, but with backscatter
689 intensity summed from the top of the HSZ at 510 mbsl to the survey ceiling at 400 mbsl. This
690 animation shows the frequency with which flares extended beyond the upper limit of the HSZ.
691 Integrated backscatter intensity and tidal data are displayed as described for animation 1.

692

693

***Highlights (for review)**

- Expulsion of free gas from Hydrate Ridge persists on decadal time scales.
- Flare intensity at 12 kHz varies strongly with time on an hourly time scale.
- Flare intensity is controlled by factors other than tidal pressure on the seafloor.
- Some flares extend above the hydrate stability zone.

Figure 1

Click here to download high resolution image

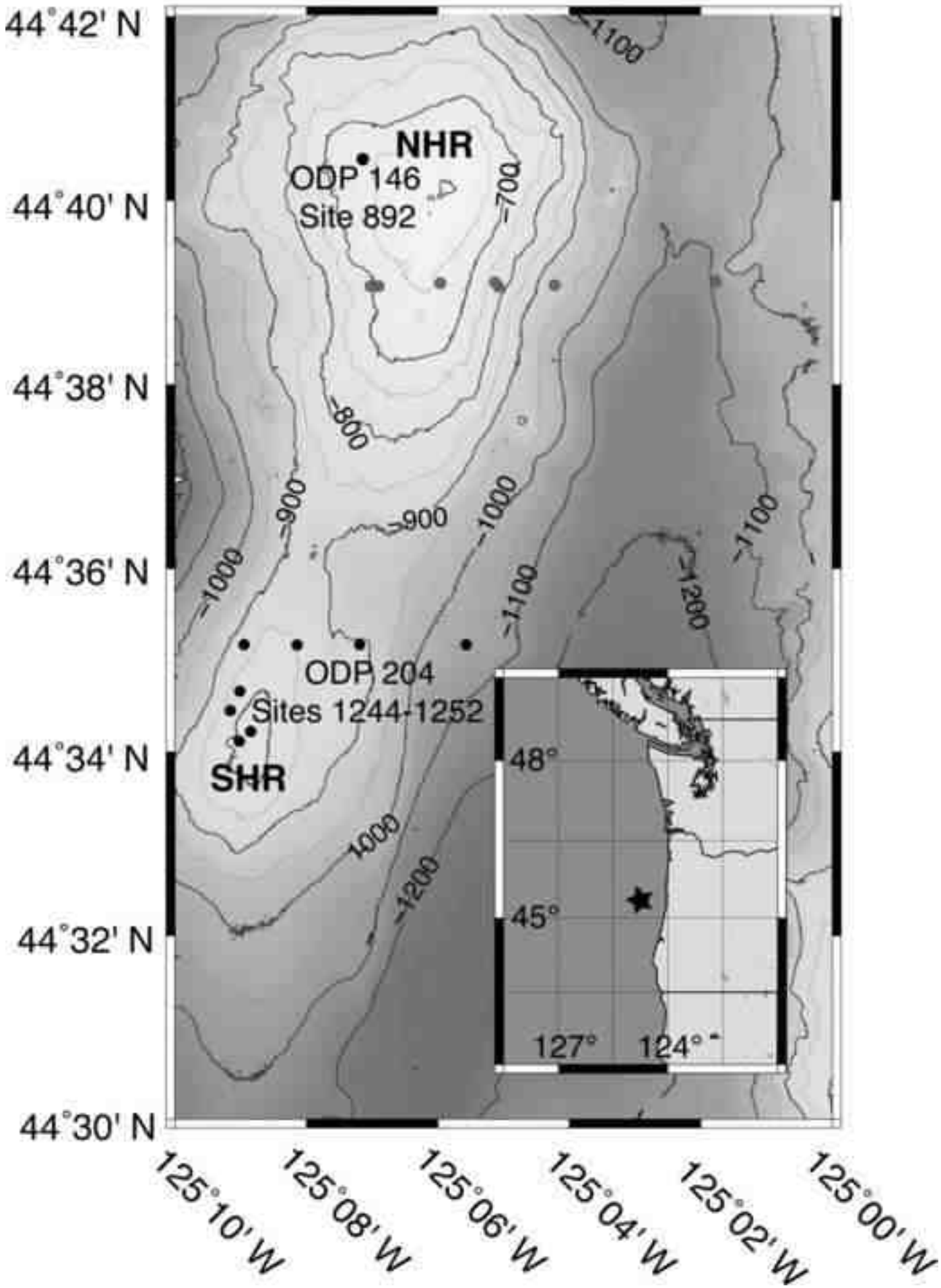

Figure 2

Click here to download high resolution image

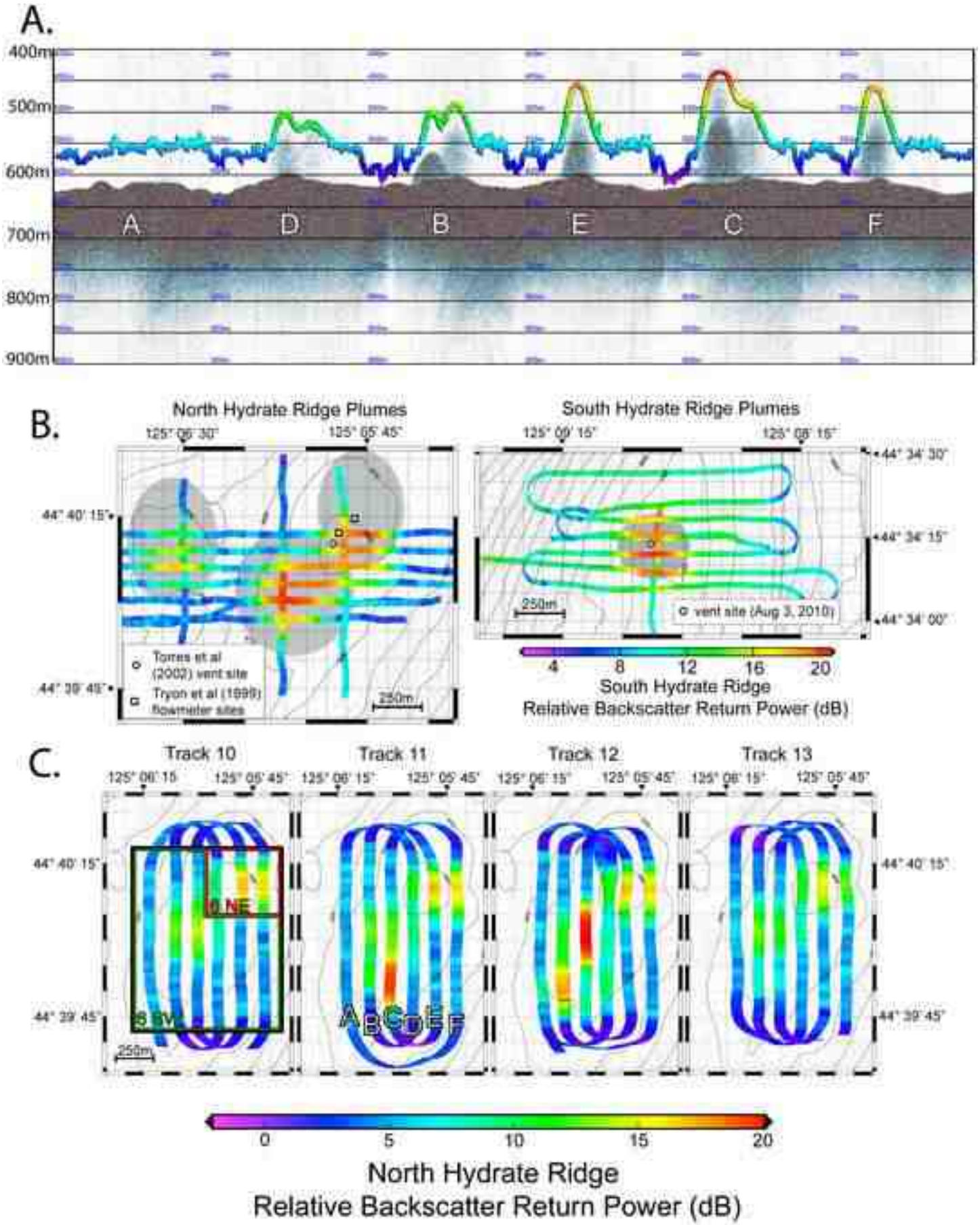

Figure 3

Click here to download Figure: Fig3_stability.pdf

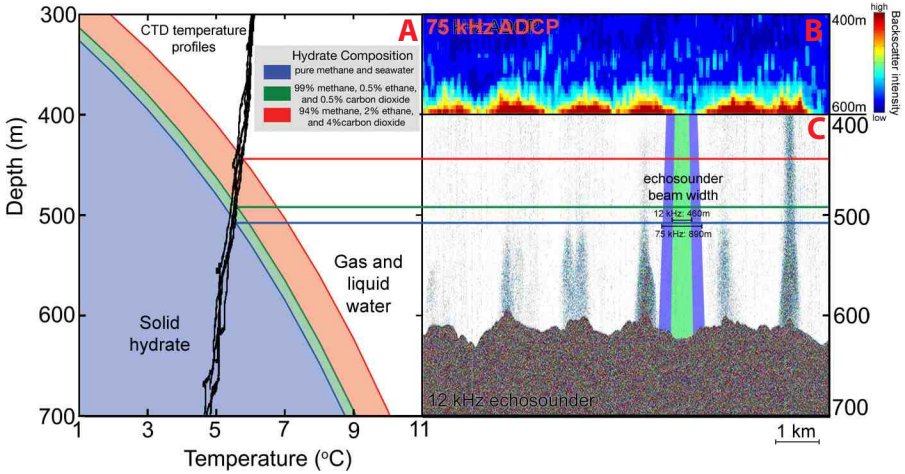

Figure 4

Click here to download high resolution image

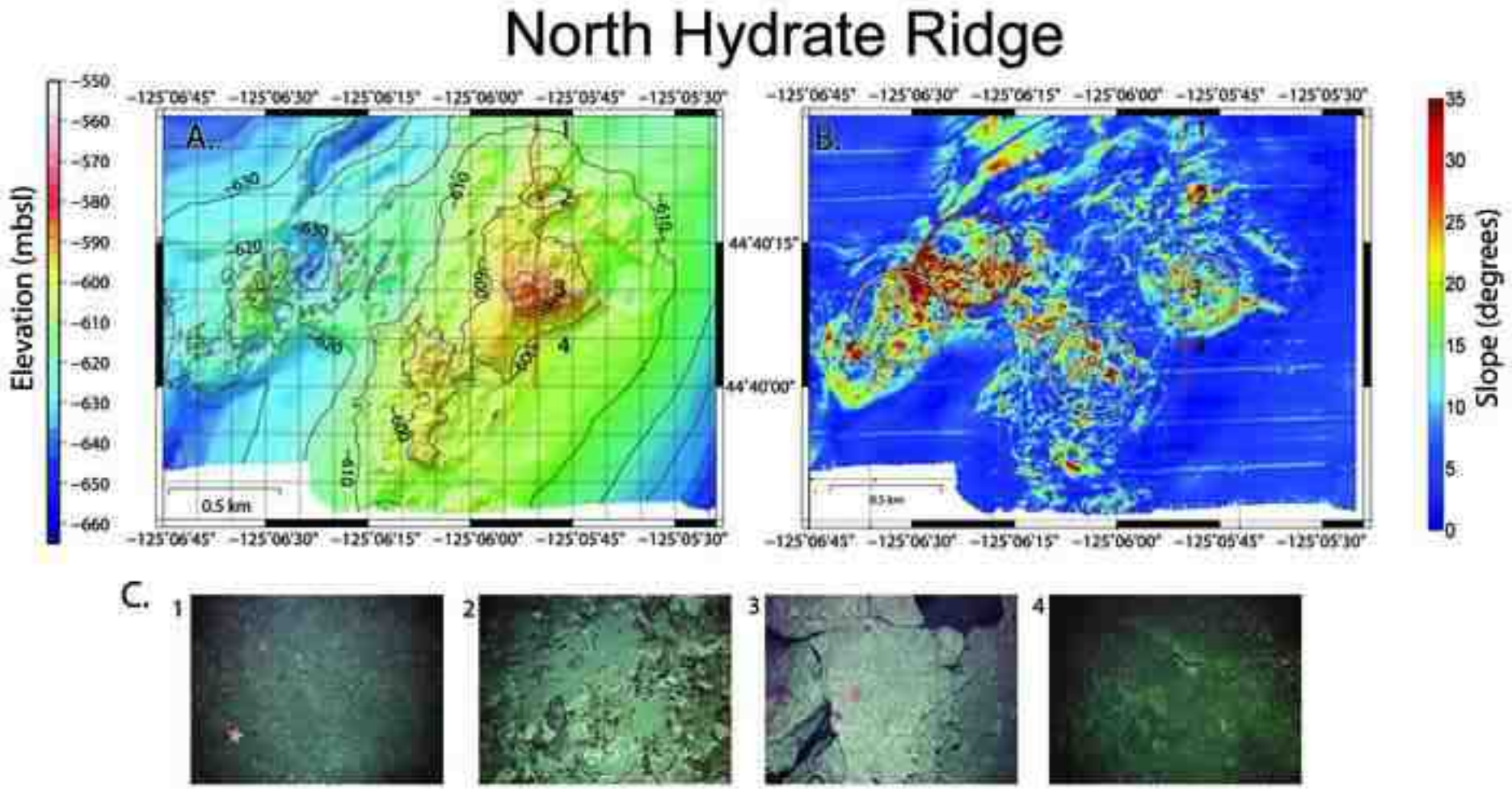

Figure 5

Click here to download high resolution image

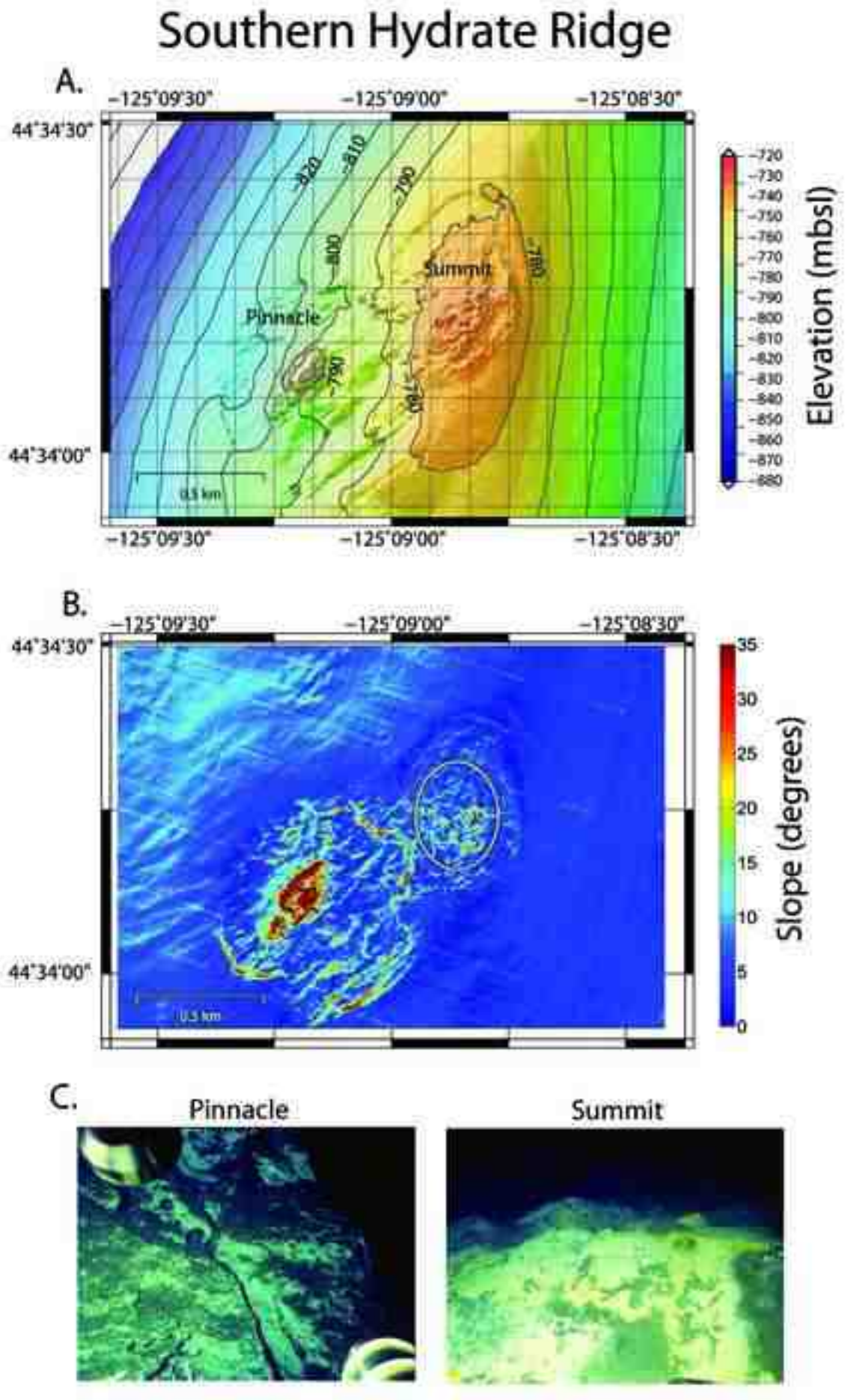

Figure 6
Click here to download Figure: Fig6.pdf

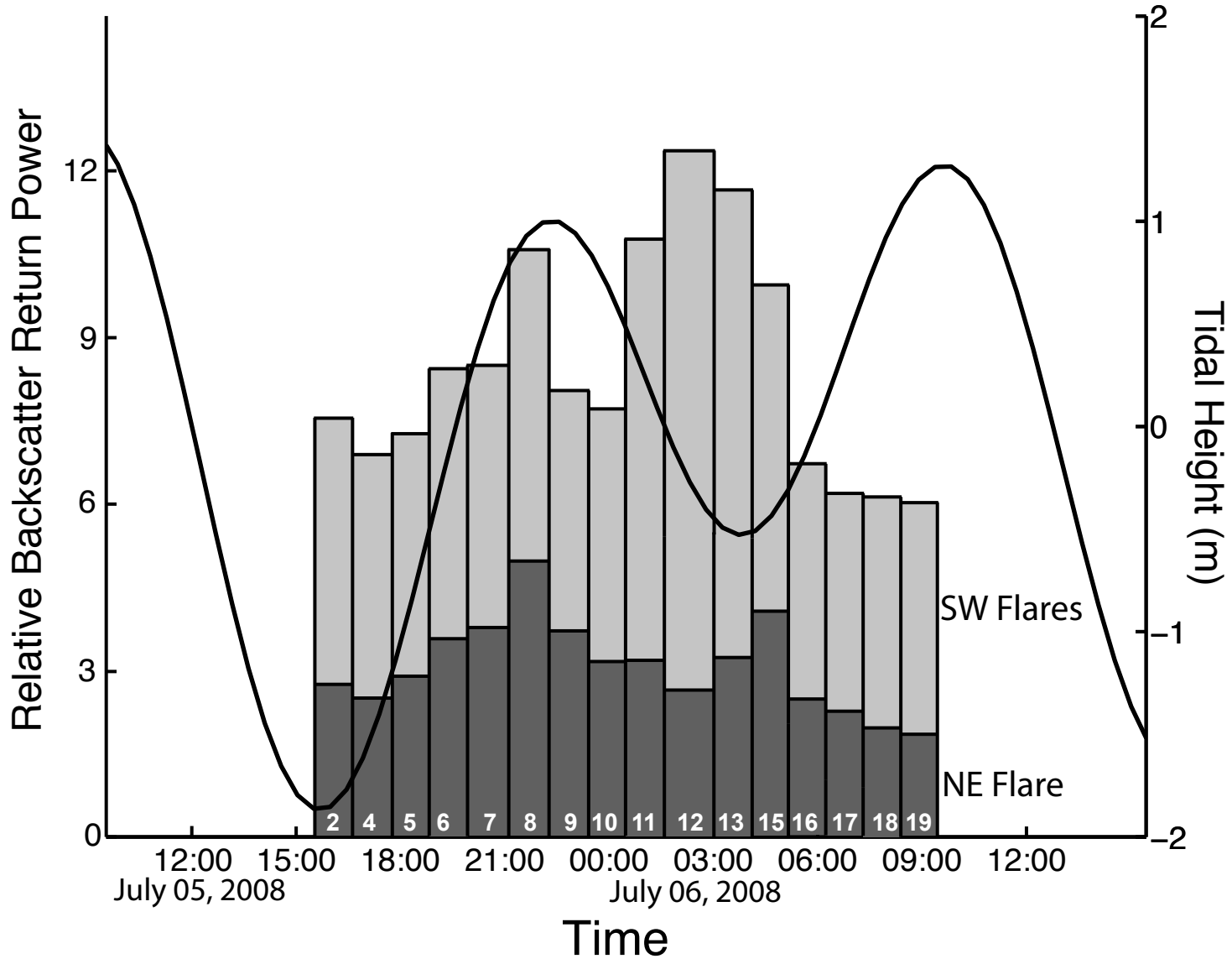

Figure 7

Click here to download high resolution image

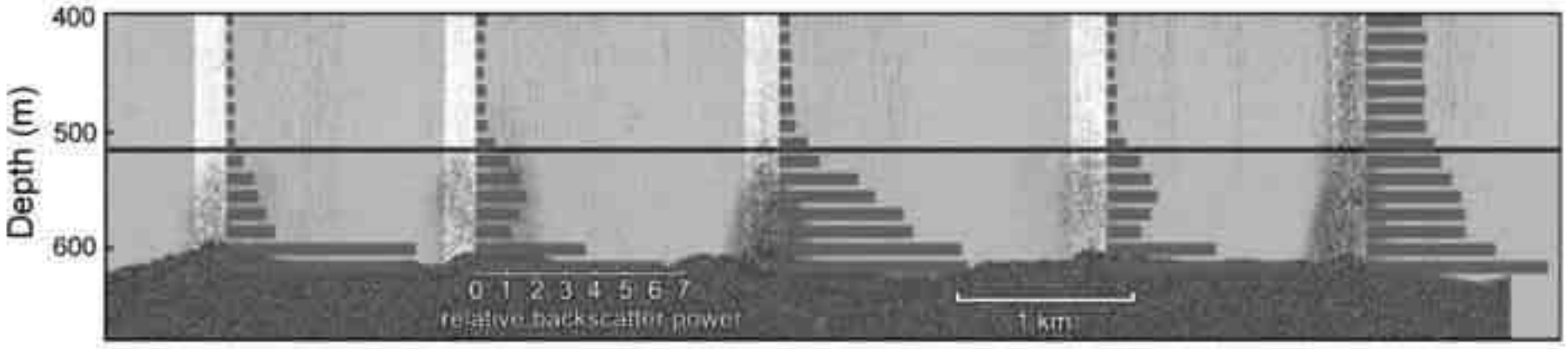

Supplementary material for on-line publication only

Click here to download Supplementary material for on-line publication only: EPSL_01136rev_supplement.pdf

Supplementary material (video)

Click here to download Supplementary material (video): kannberg.annimation1.mov

Supplementary material (video)

Click here to download Supplementary material (video): kannberg.annimation2.mov